Zeolite-Entrapped Ruthenium(II) Complexes with Bipyridine and Related Ligands. Elimination of Ligand-Field-State Deactivation and Increase in ^{3}MLCT State Lifetimes

Krzysztof Maruszewski,† Dennis P. Strommen,‡ and James R. Kincaid*,†

Contribution from the Chemistry Departments, Marquette University, Milwaukee, Wisconsin 53233, and Idaho State University, Pocatello, Idaho 83209

Received June 5, 1992

Abstract: Several homoleptic and bis-heteroleptic tris-ligated polypyridine complexes of Ru(II) have been prepared in the zeolite Y supercages. $Ru(L)_n(L')_{3-n}$–Y (where n = 0, 1, 2, 3 and L, L′ = bpy, dmb, mmb, and bpz) complexes have been investigated by electronic absorption, electronic emission, resonance Raman, and time-resolved resonance Raman spectroscopies. Excited-state lifetimes of the entrapped complexes have been measured and their temperature dependence established. While entrapment of the complexes in the zeolite matrix introduces no major modifications in structure or electron distribution, it does induce changes in the efficiency of various excited state energy dissipation pathways, the major effect being an increase in the energy of the metal-centered dd excited states which leads to elimination of one of the major decay and decomposition pathways.

Introduction

There has been an intense and sustained level of interest in the photophysical and photochemical properties of ruthenium polypyridine complexes, not only because of their value for gaining insight into the fundamental nature of primary and secondary decay processes of excited states,[1-15] but also because of their potential utility as components of practical solar energy conversion devices.[1-4] With regard to the latter issue, it is expected that development of efficient systems will require the incorporation of these or other types of sensitizer into organized assemblies which position the various components, in terms of both reactivity and spatial distribution, so as to facilitate net chemical conversion.

A most attractive approach to produce appropriately designed assemblies is to employ superstructured lattices or matrices which can serve as a framework for attachment or incorporation of the various components. Of these types of matrices, the readily available and structurally well characterized zeolites have received considerable attention.[16-18] The Y-type zeolite is of special interest with regard to the utilization of the polypyridine complexes of ruthenium because this particular zeolite structure provides "supercages" having an internal diameter (13 Å) which is sufficiently large to accommodate complexes of this size (~12 Å). In fact, early studies by Lundsford and co-workers[16] documented the convenient synthesis of tris(2,2′-bipyridine)-ruthenium(II), $Ru(bpy)_3^{2+}$, within these supercages. Once formed the chemically robust complex is entrapped within the supercage, being too large to migrate out through the (~7 Å) windows.

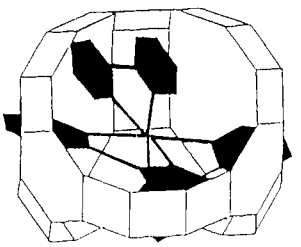

Faulkner and co-workers[19a] as well as Mallouk and co-workers[19b,c] have demonstrated photoinduced electron transfer from $Ru(bpy)_3^{2+}$ in solution to acceptors in zeolite cages. Recently, Dutta and co-workers have studied photoelectron transfer from $Ru(bpy)_3^{2+}$ to the methyl viologen dication (MV^{2+}), the latter being localized in the neighboring supercages, and have determined that the energy wasting back-electron transfer is retarded, the blue $MV^{+\bullet}$ product being stable for many hours.[18a,d] Inasmuch as it seems likely that this approach will receive further attention, it is important both to explore the synthetic versatility of this combination and to document the possible influence of the zeolite supercage cavity on the inherent properties of the complexes. In an earlier work we described a general and convenient method for the preparation of heteroleptic complexes of divalent ruthenium with various bipyridine-like ligands.[20] In the present work we report detailed studies of the photophysical

† Marquette University.
‡ Idaho State University.

(1) Kalyanasundaram, K. *Coord. Chem. Rev.* **1982**, *46*, 159.
(2) DeArmond, M. K.; Hanck, K. W.; Wertz, D. W. *Coord. Chem. Rev.* **1985**, *64*, 65.
(3) Junis, A.; Balzani, V.; Barigelletti, F.; Champagna, S.; Belser, P.; von Zelewsky, A. *Coord. Chem. Rev.* **1988**, *84*, 85.
(4) Gratzel, M. *Acc. Chem. Res.* **1981**, *14*, 376.
(5) Hager, G. D.; Crosby, G. A. *J. Am. Chem. Soc.* **1975**, *97*, 7031.
(6) Van Houten, J.; Watts, R. J. *J. Am. Chem. Soc.* **1976**, *98*, 4853.
(7) Fendler, J. H. *J. Phys. Chem.* **1985**, *89*, 2730.
(8) McClanahan, S. F.; Dallinger, R. F.; Holler, F. J.; Kincaid, J. R. *J. Am. Chem. Soc.* **1985**, *107*, 4853.
(9) Danzer, G. D.; Kincaid, J. R. *J. Phys. Chem.* **1990**, *94*, 3976.
(10) Ernst, S. D.; Kaim, W. *Inorg. Chem.* **1989**, *28*, 1520.
(11) Barigelletti, F.; De Cola, L.; Juris, A. *Gazz. Chim. Ital.* **1990**, *120*, 545.
(12) Rillema, D. P.; Allen, G.; Meyer, T. J.; Conrad, D. *Inorg. Chem.* **1983**, *22*, 1617.
(13) Allen, G. H.; White, R. P.; Rillema, D. P.; Meyer, T. J. *J. Am. Chem. Soc.* **1984**, *106*, 2613.
(14) Caspar, J. V.; Meyer, T. J. *J. Am. Chem. Soc.* **1983**, *105*, 5583.
(15) Vining, W. J.; Caspar, J. V.; Meyer, T. J. *J. Phys. Chem.* **1985**, *89*, 1099.
(16) (a) DeWilde, W.; Peeters, G.; Lunsford, J. H. *J. Phys. Chem.* **1980**, 484, 2306. (b) Quayle, W. H.; Lunsford, J. H. *Inorg. Chem.* **1982**, *21*, 97.
(17) (a) Pittit, T. L.; Fox, M. A. *J. Phys. Chem.* **1986**, *90*, 1353. (b) Collin, J. P.; Lehn, J. M.; Ziessel, R. *Nouv. J. Chim.* **1982**, *6*, 405.
(18) (a) Dutta, P. K.; Incavo, J. A. *J. Phys. Chem.* **1987**, *91*, 4443. (b) Incavo, J. A.; Dutta, P. K. *J. Phys. Chem.* **1990**, *94*, 3075. (c) Turbeville, W.; Robins, D. S.; Dutta, P. K. *J. Phys. Chem.* **1992**, *96*, 5024. (d) Dutta, P. K.; Turbeville, W. *J. Phys. Chem.* **1992**, *96*, 9410.
(19) (a) Faulkner, L. R.; Suib, S. L.; Renschler, L. L.; Green, J. M.; Bross, P. R. In *Chemistry in Energy Production*; Wymer, R. G., Keller, O. L., Eds.; ACS Symposium Series 99; American Chemical Society: Washington DC, 1982. (b) Li, Z.; Wang, C. H.; Persaud, L.; Mallouk. T. E. *J. Phys. Chem.* **1988**, *92*, 2592. (c) Kim, Y.; Mallouk, T. E. *J. Phys. Chem.* **1992**, *96*, 2879.
(20) Maruszewski, K.; Strommen, D. P.; Handrich, K.; Kincaid, J. R. *Inorg. Chem.* **1991**, *30*, 4579.

0002-7863/93/1515-8345$04.00/0

properties of such systems which demonstrate that while the structural features of the complexes remain relatively unperturbed, dramatic effects on the ^{3}MLCT excited-state lifetimes are induced by entrapment within the zeolite-Y supercage.

Experimental Section

A. Materials. The Y zeolite was generously provided by the Union Carbide Corp., Danbury, CT. $Ru(NH_3)_6Cl_3$, 2,2′-bipyridine (bpy), 4,4′-dimethyl-2,2′-bipyridine (dmb), and 2,2′-bipyrazine (bpz) were purchased from the Aldrich Chemical Co., Milwaukee, WI. The ligands were sublimed prior to use. The synthesis of 4-monomethyl-2,2′-bipyridine (mmb) will be described in a forthcoming paper.[21]

B. Preparation of Compounds. The syntheses of zeolite-entrapped complexes $Ru(bpy)_3^{2+}$–Y, $Ru(bpy)_2(bpz)^{2+}$–Y, and $Ru(bpy)_2(dmb)^{2+}$–Y have been described previously[20] and $Ru(bpz)_3^{2+}$–Y was prepared by analogous procedures. All physical measurements with the exception of excited-state lifetime measurements were conducted on samples prepared as described in ref 20. In order to avoid concentration quenching, samples having a 10 times lower concentration (2.5 mg of $Ru(NH_3)_6^{3+}$ per 1 g of zeolite) of ruthenium complex were employed for excited-state lifetime measurements. The zeolite-entrapped complexes were extracted from the zeolite matrix by methods described in ref 20. The integrity of each sample was confirmed as described previously[20] by RR, electronic absorption, and emission spectra as well as by luminescence lifetime measurements. We wish to point out that in the case of $Ru(bpy)_2(bpz)$–Y trace amounts of $Ru(bpy)_3$–Y were formed, presumably as a consequence of incomplete removal of free bipyridine from the $Ru(bpy)_2$–Y precursor complex. However, the presence of this low-level contaminant has no effect on the observed lifetime of the target complex inasmuch as the emission maxima are quite well separated.

C. Spectroscopic Measurements. 1. Electronic Absorption Spectra. Electronic absorption spectra were obtained with a Hewlett-Packard Model 8452A diode array spectrometer. Solid samples were mixed with a few drops of mineral oil and the resulting paste was diluted with additional oil and placed in a 1-cm quartz cuvette. Spectra were obtained in the absorbance mode.

2. Ground-State Resonance Raman Spectra. Spectra were obtained with a conventional Raman spectrometer (Spex Model 1403 double monochromator equipped with a Spex Model DM1B controller and a Hamamatsu R928 photomultiplier tube) with 457.9-nm excitation from a Spectra-Physics Model 2025-05 argon ion laser. Excitation at 441.7 nm was provided by a Liconix Model 4240NB He–Cd laser, while 406.7- and 356.4-nm excitations were obtained from a Coherent Model Innova-100-K3 krypton ion laser. Spectra of the zeolite-entrapped compounds were obtained from solid samples in rotating NMR tubes. Spectra of the compounds extracted from the zeolite matrix were obtained from aqueous solutions in the same manner. The laser beams, except 356.4-nm excitation, were focused onto the sample by using a glass lens, and the scattered light was collected with use of a 135° backscattering geometry and a conventional two-lens (glass) collecting system. Quartz lenses were employed for obtaining resonance Raman spectra with the 356.4-nm excitation line.

3. Time-Resolved ^{3}MLCT Resonance Raman Spectra. Excited-state Raman spectra were obtained with use of the spectrophotometer and detector described above. The third harmonic (354.7 nm) from a Quanta-Ray (Spectra-Physics) Model DCR-3 Nd:YAG laser (operated at 20 Hz) was used as an excitation source. The photomultiplier tube output signal was directed to a Stanford Research Systems (SRS) Model SR240 fast preamplifier and then averaged by an SRS Model SR250 gated integrator and boxcar averager. The boxcar was triggered by the pretrigger output of the Nd:YAG laser and, typically, 50 events were averaged per point. The averaged output was passed through a locally constructed voltage-to-frequency converter (analogous to the Spex Model DM103) and acquired by a Spex Model DM1B controller. Samples of zeolite-entrapped complexes were placed in NMR tubes, immersed in deionized water, and degassed by purging with N_2 for ca. 30 min. Spectra were collected by using rotating NMR tubes in the scattering geometry described above. Spectra of the compounds extracted from the zeolite matrix were obtained from water solutions in the same manner.

D. Emission Spectra. The collection apparatus was the same as for the ground-state Raman measurements. Typically, 457.9-nm excitation was focused onto the spun NMR tubes containing solid samples of zeolite-entrapped complexes. Emission spectra were recorded with 10-cm^{-1} increments. Spectra of the compounds extracted from the zeolite matrix were obtained from water solutions in the same manner. The emission spectra were not corrected for spectrometer response.

E. Excited-State Lifetimes. Lifetimes were obtained by using a Spex Model 1401 double monochromator equipped with a Spex Model DM1B controller and an RCA C31034A-02 photomultiplier tube. The 354.7-nm radiation from a Quanta-Ray (Spectra-Physics) Model DCR-3 Nd:YAG laser (operated at 20 Hz) was used as the excitation source with the beam defocused. The photomultiplier tube output signal was directed to a SRS Model SR250 gated integrator and boxcar averager. The boxcar was triggered by the pretrigger output of the Nd:YAG laser, typically, 40 events per point. The boxcar gate was moved on the time scale by a voltage ramp generated as an output by a Spex Model DM1B controller. The averaged output was passed through a locally constructed voltage-to-frequency converter (analogous to the Spex Model DM103) and acquired by a Spex Model DM1B controller. Typically, decay curves were collected up to 10 μs after the initial laser pulse. The background (dark current) signal was subtracted from the recorded curve in order to remove electronic ringing induced by the integrator/averager module. Decay curves were fitted (within ca. 4τ) into monoexponential curves by a locally written computer program. In those cases where the obtained fits were not satisfactory, a biexponential function was used in order to resolve the dominant decay curve.

The excited-state lifetimes were acquired at various temperatures with the aid of a cold cell of in-house design, which consists of a dewar containing an NMR tube spinner. The spinning NMR tube and a low-temperature thermometer are placed at equal distances from a jet from which cold nitrogen gas is emitted. The temperature was controlled (±1 °C) by adjusting of rate of cold nitrogen gas flow.

Results and Discussion

A. Synthetic Aspects of Intrazeolite Chemistry. The steric and electrostatic restrictions imposed by the zeolite host result in significant limitations in the types of complexes that can be prepared within the supercage. Thus, we were unable to prepare $Ru(dmb)_3^{2+}$–Y even when heating Ru^{III}–Y with dmb at high temperatures for extended periods of time. The only product that could be detected was $Ru(dmb)_2^{2+}$–Y indicating that the tris complex is too large to be accommondate by the (13 Å) zeolite supercage.

During the high-temperature preparation of tris-heteroleptic complexes of Ru(II) from the zeolite-entrapped bis-ligated precursors, the possibility exists that ligand exchange or modification might occur, thus converting the bis species to unwanted tris-ligated heteroleptic complexes. For example, $Ru(dmb)_2^{2+}$–Y was heated at 190 °C for 12 h with bpy in an attempt to obtain $Ru(dmb)_2(bpy)^{2+}$–Y. However, the resonance Raman spectrum of the product was virtually identical with the spectrum of $Ru(bpy)_2(dmb)^{2+}$–Y. Inasmuch as the intensities of the dmb Raman bands are smaller than those of bpy and there is some overlap,[8] small zeolite matrix effects could be invoked to account for the weakness of the dmb features in the spectrum. However, the resonance Raman spectrum of the complex extracted from the zeolite matrix is virtually identical with the spectrum of independently prepared $Ru(bpy)_2(dmb)^{2+}$ and significantly different from that of an authentic sample of $Ru(dmb)_2(bpy)^{2+}$. Figure 1 shows these three resonance Raman spectra obtained with MLCT excitation. Several regions of the spectra are useful to evaluate purity. For example, the bpy ligand exhibits a band at 1608 cm^{-1} while the corresponding dmb band occurs[8] at 1623 cm^{-1}. Thus, as can be seen from inspection of Figure 1, the spectrum of pure $Ru(bpy)(dmb)_2^{2+}$ (trace C) exhibits significantly larger intensity at 1623 cm^{-1}.

With respect to bpz complexes we were able to synthesize both $Ru(bpy)_2(bpz)^{2+}$–Y and $Ru(bpz)_3^{2+}$–Y complexes. However, it proved impossible to obtain pure $Ru(bpz)_2^{2+}$–Y. Electronic absorption spectra of the reaction products showed that $Ru(bpz)_2^{2+}$–Y was substantially contaminated with an unidentified substance. Thus aqueous solutions of pure $Ru(bpz)_2^{2+}$ exhibit a single symmetric absorption band at 520 nm,[3] but the entrapped

(21) Treffert-Zemelis, S. M.; Golus, J.; Strommen, D. P.; Kincaid, J. R. *Inorg. Chem.*, in press.

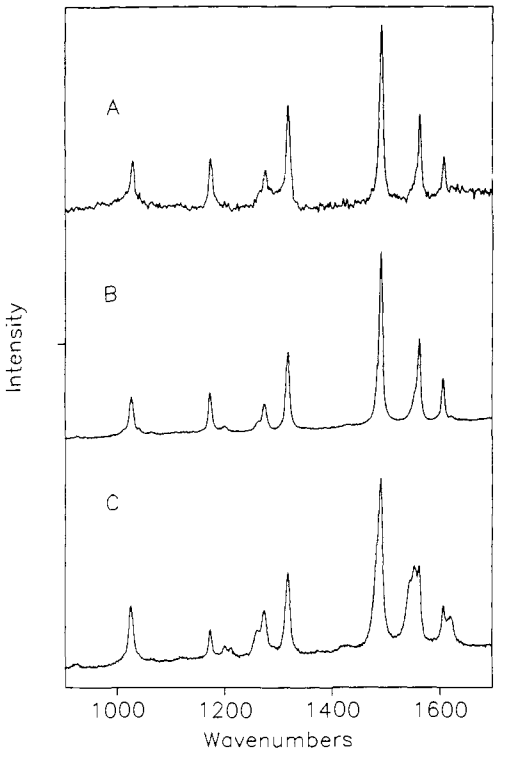

Figure 1. Resonance Raman spectra (with 457.9-nm excitation) of $Ru(bpy)_2(dmb)^{2+}$ extracted from zeolite (trace A), independently prepared $Ru(bpy)_2(dmb)^{2+}$ (trace B), and independently prepared $Ru(dmb)_2(bpy)^{2+}$ (trace C).

complex exhibits a second band at 480 nm. Futhermore, extracts of this sample also contained the 480-nm band ascribable to this unidentified impurity (with essentially comparable relative intensities). When such a sample was heated at high temperature with bpy, the resonance Raman spectrum of the product showed anomalously large intensities for bpy bands. However, the contaminated $Ru(bpz)_2^{2+}$–Y can be converted to pure $Ru(bpz)_3^{2+}$–Y when reacted with excess bpz at elevated temperatures.

B. Electronic Absorption and Emission Spectra. The electronic absorption and emission spectra of most of the complexes studied exhibit slight red shifts in the observed maxima (only several hundred wavenumbers). The electronic absorption spectra of zeolite-entrapped and free $Ru(mmb)_3^{2+}$ are shown in Figure 2 and are typical of those obtained for other complexes. Similarly, Figure 3 illustrates typical emission spectra of zeolite-entrapped and free $Ru(bpy)_2(bpz)^{2+}$. Table I summarizes the electronic absorption and emission maxima for the free and entrapped complexes.

Inspection of the table shows that while in most cases slight red shifts in both absorption and emission maxima are observed, two of the complexes, $Ru(bpy)_2(bpz)^{2+}$ and $Ru(bpz)_3^{2+}$, are blue-shifted. The significance of these spectral changes in terms of "energy-gap law" effects on lifetime is discussed in a later section.

C. Ground-State Resonance Raman Spectra. The observed frequencies for all compounds studied are shown in Table II. While the ground-state spectral pattern does not significantly change upon incorporation of the complexes into the zeolite matrix, significant frequency shifts in some bands are observed. Thus, in the low-frequency region (between 400 and 200 cm^{-1}), wherein observed features are expected to contain substantial contribution from ν(Ru–N), rather large shifts ($\sim$10 cm^{-1}) are observed. In contrast, much smaller relative changes in frequencies are observed for modes in the higher energy region (between 700 and 1700 cm^{-1}).

D. Time-Resolved ^{3}MLCT Resonance Raman Spectra. It has been shown that upon ^{3}MLCT state formation, the photoelectron

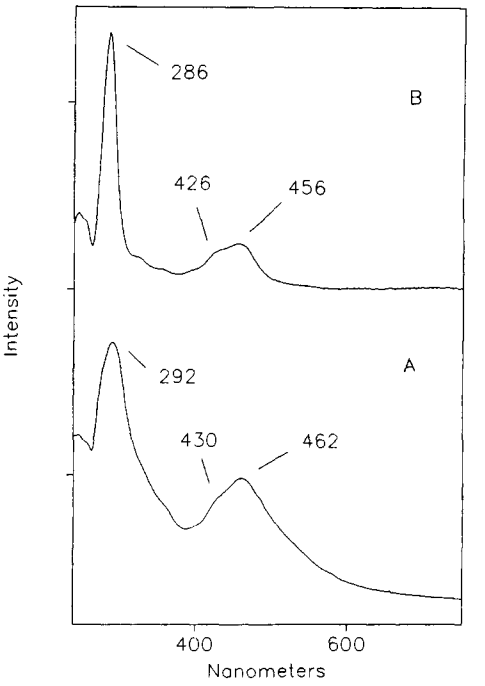

Figure 2. Electronic spectra of a Nujol suspension of $Ru(mmb)_3^{2+}$–Y (trace A) and an aqueous solution of independently synthesized complex (trace B).

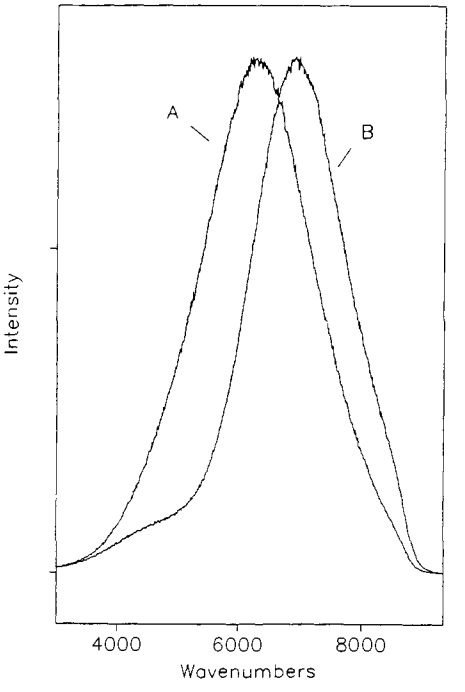

Figure 3. Electronic emission spectra of $Ru(bpy)_2(bpz)^{2+}$–Y (trace A) and an aqueous solution of independently synthesized complex (trace B).

is localized on a single ligand molecule.[8,22-25] Thus one can expect a large dipole moment to be present in the ^{3}MLCT excited state.[26] In addition, when a ligand molecule accommodates a photoelectron, it is expected to undergo structural changes.[27] These assumptions might indicate strong interactions, both electrostatic

(22) Bradley, P. G.; Kress, N.; Hornberg, B. A.; Dallinger, R. F.; Woodruft, W. H. *J. Am. Chem. Soc.* **1981**, *103*, 7441.
(23) Dallinger, R. F.; Woodruff, W. H. *J. Am. Chem. Soc.* **1979**, *101*, 4391.
(24) Sutin, N.; Creutz, C. *Adv. Chem. Ser.* **1978**, *168*, 1.
(25) Heath, G. A.; Yellowlees, C. J.; Braterman, P. S. *J. Chem. Soc., Chem. Commun.* **1981**, 287.
(26) Kober, E. M.; Sullivan, B. P.; Meyer, T. J. *Inorg. Chem.* **1984**, *23*, 2098.

Table I. Absorption Maxima, Emission Maxima, and Excited-State Lifetimes for Zeolite-Entrapped and Solutions of Ru(II) Polypyridine Complexes

compd	absorption (max),[a] nm		emission (max), nm			lifetime, ns		
	Z[b]	H_2O	Z	H_2O	PC[c]	Z	H_2O	PC
$Ru(bpy)_3^{2+}$	286/432, 456	287/426, 452	618	609	620	530	600	868
$Ru(bpy)_2(dmb)^{2+}$	288/429, 464	287/428, 456	623	618		506	501	
$Ru(mmb)_3^{2+}$	292/430, 462	286/426, 456	630	615		368	513	
$Ru(bpz)_3^{2+}$	292/446	295/443	595	600	610	1433	853	846
$Ru(bpy)_2(bpz)^{2+}$	282/410, 480	282/406, 485	674	705	710	344	127	353

[a] $\pi \rightarrow \pi^*/d\pi \rightarrow \pi^*$ transitions. [b] Zeolite entrapped. [c] Propylene carbonate; data from ref 13.

Table II. Comparison of Resonance Raman Frequencies (cm^{-1}) for Zeolite-Entrapped and Aqueous Solutions of Ru(II) Polypyridine Complexes Obtained with MLCT Excitations

$Ru(bpy)_3^{2+}$		$Ru(bpy)_2(dmb)^{2+}$		$Ru(mmb)_3^{2+}$		$Ru(bpz)_3^{2+}$		$Ru(bpy)_2(bpz)^{2+}$	
Z	H_2O	Z	H_2O	Z	H_2O	Z	H_2O	Z	H_2O
1611	1608	1616[a]	1621	1622[a]	1621	1593	1596	1610	1606
1564	1563	1605	1607	1613	1608	1517	1517	1591	1594
1493	1491	1564	1563	1566	1567	1483	1486	1567	1564
1322	1320	1559	1556	1556	1556	1408	1410	1514	1511
1273	1276	1490	1491	1491	1489	1338	1346	1497	1492
1179	1176	1320	1320	1327	1323	1276	1277	1409	1408
1048[a]	1043	1274	1277	1272	1276	1195	1194	1340	1346
1032	1028	1263[a]	1263		1261	1167	1164	1321	1320
672	668		1202	1214	1212	1054	1051	1274	1278
377	370	1176	1175	1173	1167	1026	1028		1270
346	340	1048[a]	1043	1045[a]	1042	802	802	1195	1191
	283	1029	1026	1029	1028	676	679	1181	1176
			745	886	885	663	666	1170	1164
		672	668	749	748	377	379	1040	1035
			566	731	732[a]	347	340	802	804
		376	372	664	668		275	675	675
		356[a]	359	564	565			381	378
		340	329	378	367			354	339
				363	362				
				323	323				
				298	295				

[a] Shoulder.

and steric, between a guest molecule in its excited state and the zeolite supercage wall. However, the observed TR^3 spectra of the zeolite-entrapped complexes show only minor changes compared to those of the solution species. For all of the tris-heteroleptic complexes that we investigated we were able to confirm that the photoelectron was localized on the same ligand as for the free molecules. Thus, for $Ru(bpy)_2(dmb)^{2+}$–Y the photoelectron is localized on bpy and in the case of $Ru(bpy)_2(bpz)^{2+}$–Y it is localized on the bpz ligand.

Figure 4 shows a typical TR^3 spectrum of $Ru(bpy)_2(bpz)^{2+}$–Y compared with a spectrum of $Ru(bpy)_2(bpz)^{2+}$ extracted from the zeolite matrix. In the case of the TR^3 spectra collected from the zeolite-entrapped complexes we were unable to obtain complete saturation of the excited state as we were in the case of water solutions of the complexes. High laser powers cause zeolite destruction as evidenced by changes in sample color and gradual appearance of an orange color in the aqueous phase of the zeolite suspension.

E. Excited-State Lifetimes. 1. Photophysics of Excited Electronic States of Ru(II) Polypyridine Complexes. The deactivation pathways whose efficiencies determine the observed excited-state lifetimes of Ru(II) polypyridine complexes are presented in Scheme I. Population of three closely spaced[29] triplet MLCT states follows excitation in the visible region (^{1}MLCT) and occurs with very high quantum yield ($\phi_{isc} \approx 1$).[32] Deactivation of the cluster of emitting triplet states can take place via radiative decay (k_r), non-radiative decay (k_{nr}), and thermal population of metal-localized triplet states (^{3}dd). It has been shown that in some cases another ligand-localized triplet state, higher in energy by a few hundred wavenumbers, serves as an additional energy dissipation channel.[13,30,31]

The excited-state lifetime (τ) is equal to the reciprocal of the total deactivation rate constant (k_{tot}) which is shown by

$$k_{tot} = k_r + k_{nr} + k_1 \exp(-\Delta E_1/kT) + k_2 \exp(-\Delta E_2/kT) \quad (1)$$

The deactivation rate constant of the thermally populated metal-localized (^{3}dd) states is designated k_1. Population of ^{3}dd state leads to fast nonradiative decay to ground state (k_{dd}) or to ligand loss (k_{rx}). ΔE_1 is the energy gap between the ^{3}dd states and the cluster of ^{3}MLCT emitting states. The deactivation rate constant, k_2, is associated with the additional ^{3}MLCT state which may be thermally populated due to the small magnitude of ΔE_2.

Figure 5 shows typical curves obtained for the luminescence lifetime measurements at room temperature. In order to determine the values of the various kinetic parameters contained in eq 1, it is necessary to conduct lifetime measurements over a range of temperatures. This was done for all of the complexes studied, and the resulting kinetic parameters are given in Table III along with those obtained by Meyer and co-workers[13,30] for the same complexes (where available) in different media.

It has been observed[18b] that in some cases the decay curves obtained for $Ru(bpy)_3^{2+}$ in zeolite Y exhibit biexponential

(27) Mallick, P. K.; Strommen, D. P.; Kincaid, J. R. *J. Am. Chem. Soc.* **1990**, *112*, 1686.
(28) Caspar, J. V.; Sullivan, B. P.; Kober, E. M.; Meyer, T. J. *Chem. Phys. Lett.* **1982**, *91*, 91.
(29) Kober, E. M.; Meyer, T. J. *Inorg. Chem.* **1984**, *23*, 3877.
(30) Lumpkin, R. S.; Kober, E. M.; Worl, L. A.; Murtaza, Z.; Meyer, T. J. *J. Phys. Chem.* **1990**, *94*, 239.
(31) Rillema, D. P.; Blanton, C. B.; Shaver, R. J.; Jackman, D. C.; Boldaji, M.; Bundy, S.; Worl, L. A.; Meyer, T. J. *Inorg. Chem.* **1992**, *31*, 1600.
(32) Bolletta, F.; Juris, A.; Maestri, M.; Sandrini, D. *Inorg. Chem. Acta* **1980**, *41*, 1175.
(33) Mines, G. A.; Roberts, J. A.; Hupp, J. T. *Inorg. Chem.* **1992**, *31*, 125.

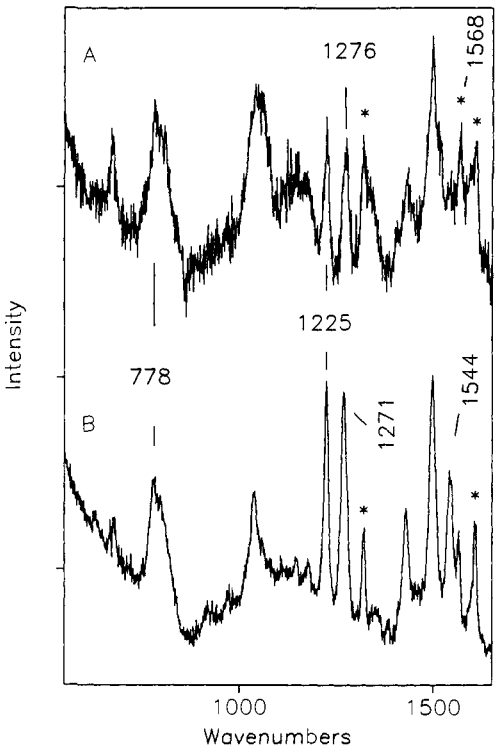

Figure 4. Time-resolved Raman (TR^3) spectra of Ru(bpy)$_2$(bpz)$^{2+}$ with 354.7-nm excitation: zeolite-entrapped complex (trace A) and independently synthesized complex (trace B). Asterisks denote bands of neutral bpy ligands.

Scheme I. Diagram of the Excited-State Deactivation Pathways in Ru(bpy)$_3^{2+}$

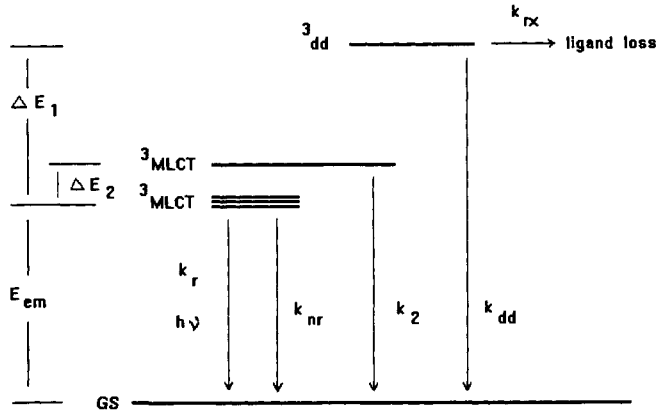

behavior. In the case of the zeolite-entrapped Ru(bpy)$_3^{2+}$, Ru(bpy)$_2$(dmb)$^{2+}$, Ru(bpy)$_2$(bpz)$^{2+}$ and Ru(mmb)$_3^{2+}$ complexes the decay curves exhibit monoexponential behavior at room temperature. However, the zeolite-entrapped Ru(bpz)$_3^{2+}$ complex exhibits biexponential behavior with the lifetime of the short-living component being equal to 330 ns (30% of the initial counts). Furthermore, at low temperatures the decay curves for all investigated compounds show biexponential behavior with approximately 30% weights of the short-living component in the calculated curves.

Before proceeding to a discussion of the data for the zeolite-entrapped complexes, it is useful to briefly summarize the results for Ru(bpy)$_3^{2+}$ in solution (propylene carbonate, PC) and in a rigid cellulose acetate (CA) matrix. The curves illustrating the temperature dependence of the lifetimes for these two cases and for zeolite-entrapped Ru(bpy)$_3^{2+}$ are given in Figure 6. Meyer and co-workers obtained the parameters given in Table III by applying an expression similar to eq 1, pointing out that only a single exponential term is required, in both cases, to

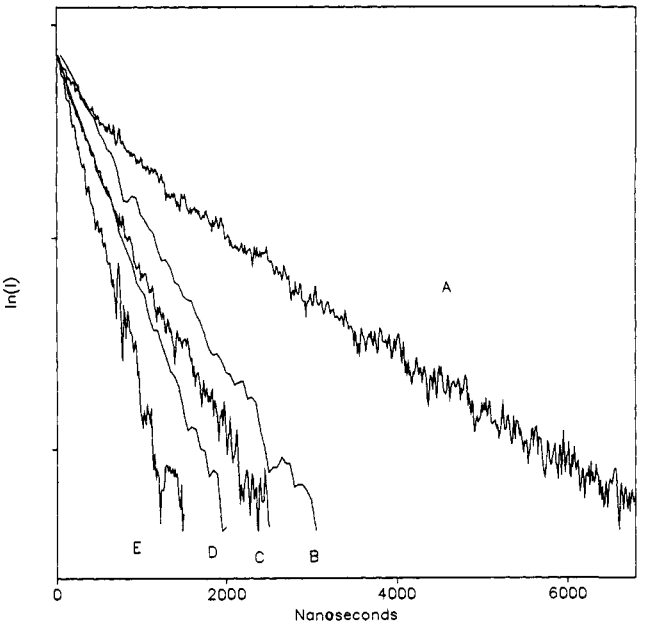

Figure 5. Excited electronic state decay curves obtained at room temperature for zeolite-entrapped Ru(bpz)$_3^{2+}$ (trace A), Ru(bpy)$_3^{2+}$ (trace B), Ru(bpy)$_2$(dmb)$^{2+}$ (trace C), Ru(mmb)$_3^{2+}$ (trace D), and Ru(bpy)$_2$(bpz)$^{2+}$ (trace E).

Table III. Kinetic Decay Parameters for Ru(II) Polypyridine Complexes

compd	$k_r + k_{nr}$, s^{-1} × 10^5	k_1, s^{-1} × 10^{12}	ΔE_1, cm^{-1}	k_2, s^{-1} × 10^7	ΔE_2, cm^{-1}
Ru(bpy)$_3^{2+}$-Z[a]	3.8			11	890
Ru(bpy)$_3^{2+}$-CA[b]	10			1.7	810
Ru(bpy)$_3^{2+}$-PC[c]	6.1	4	3275		
Ru(bpy)$_2$(dmb)-Z	4.3			6.8	777
Ru(mmb)$_3$-Z	4.3			2.9	533
Ru(bpz)$_3^{2+}$-Z	4.1			1.1	765
Ru(bpz)$_3^{2+}$-PC	3.3	8	3325		
Ru(bpy)$_2$(bpz)$^{2+}$-Z	5.4			19	894
Ru(bpy)$_2$(bpz)$^{2+}$-PC	21			3	800

[a] Complex entrapped in zeolite. [b] In cellulose acetate; data from ref 30. [c] In propylene carbonate; data from ref 13.

fit the data; i.e.,

$$k_{tot} = k_r + k_{nr} + k' \exp(-\Delta E'/kT) \qquad (2)$$

where, k' (and $\Delta E'$) corresponds to *either* k_1 or k_2 (ΔE_1 or ΔE_2) in equ 1.

As can be seen by referring to Figure 6 and Table III, the effect of incorporation of Ru(bpy)$_3^{2+}$ into a rigid cellulose acetate matrix has a rather dramatic effect on the temperature dependence of the lifetime. The analyses of the two curves, using eq 2, shows that the major effect of the cellulose acetate matrix is to markedly change the parameters included in the temperature-dependent term. In the case of Ru(bpy)$_3^{2+}$ in PC solution the $\Delta E'$ value is 3275 cm^{-1} and the pre-exponential factor has a value of 4 × 10^{12} s^{-1}, whereas the corresponding values for cellulose acetate are 810 cm^{-1} and 1.7 × 10^7 s^{-1}.

These large differences obviously imply different thermally activated decay pathways, and Meyer and co-workers[13] provided convincing arguments that these two pathways are associated with decay through the dd^3 excited states (Ru(bpy)$_3^{2+}$ in PC solution) or through population of an additional MLCT state positioned approximately 800 cm^{-1} above the manifold of the three lowest energy ^{3}MLCT states (in the case of Ru(bpy)$_3^{2+}$ in cellulose acetate). Thus, the effect of incorporation of Ru(bpy)$_3^{2+}$ into the rigid cellulose acetate matrix is to inhibit decay through the dd pathway, and the temperature dependence is then dominanted by thermal activation of the decay through the

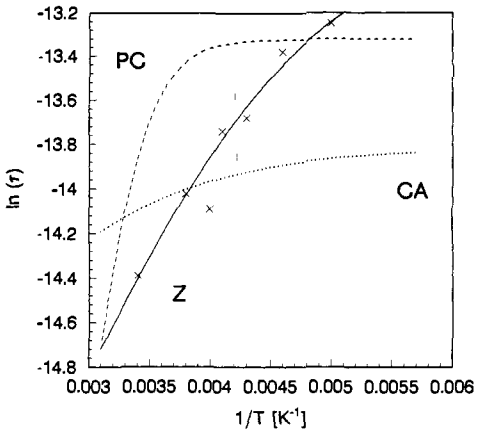

Figure 6. Comparison of the temperature-dependent lifetime data obtained for $Ru(bpy)_3^{2+}$ in propylene carbonate (PC) (ref 13) and cellulose acetate (CA) (ref 30) and entrapped in zeolite (Z). The experimental points are marked by ×. The solid lines for the PA and CA samples were generated from eq 2 by using the parameters given in refs 13 and 30, respectively. The solid line for $Ru(bpy)_3^{2+}$–Y represents the best fit for eq 2 and results in the parameters given in Table III.

additional MLCT state. As Meyer and co-workers point out, this inhibition of the dd decay pathway is entirely reasonable, given the nature of the ^{3}dd excited state. Thus, population of this state is expected to lead to elongation of the Ru–N bonds. In the rigid cellulose acetate matrix such distortions are inhibited so that the energy of this state in the cellulose acetate matrix is expected to be increased (i.e., the ΔE_1 value will increase). Apparently, the magnitude of the increase is sufficient to eliminate the contribution of this decay pathway to the overall decay process.

2. Effects of Zeolite Entrapment on the Lifetimes of Ru(II) Polypyridine Complexes. As can be seen by inspection of Figure 6, the shape of the temperature-dependent lifetime curve of $Ru(bpy)_3^{2+}$–Y is dramatically altered compared to that in solution and, in fact, the ΔE value extracted from this curve is quite similar to that obtained for $Ru(bpy)_3^{2+}$ in cellulose acetate. The obvious implication of this result is that entrapment of $Ru(bpy)_3^{2+}$ within the zeolite supercage also leads to increases in the energy of the ^{3}dd state and eliminates this decay pathway. It seems worth pointing out that some evidence for distortion of the Ru–N bonds of the entrapped complexes is provided by the observed increases ($\sim$10 cm^{-1}) in the low-frequency (200–400 cm^{-1}) RR modes which are expected to contain significant contributions from the Ru–N coordinates.

The kinetic parameters for all of the complexes studied are given in Table III. In all cases it is seen that the ΔE and pre-exponential factors extracted from the curves are consistent with elimination of the ^{3}dd decay pathway. In fact, all of the ΔE values lie between 500 and 900 cm^{-1}, similar to the range of results observed in the few complexes previously shown to exhibit non-active ligand-field decay.[13,30]

General agreement with expectations based on energy gap law is noted for the linear term in the various complexes for which such a comparison is valid (i.e., where the ^{3}MLCT state is localized on a given ligand). Thus, both $Ru(bpy)_3^{2+}$–Y and $Ru(bpy)_2(dmb)^{2+}$–Y possess bpy localized ^{3}MLCT states[8] and the linear terms ($k_r + k_{nr}$) are 3.8×10^5 and 4.3×10^5 s^{-1} for λ_{max} values of 618 and 623 nm, respectively. Similar agreement is noted for the two bipyrazine-containing complexes. Thus, $Ru(bpy)_2(bpz)^{2+}$–Y, which emits at 674 nm, has a linear term equal to 5.4×10^5 s^{-1}, whereas $Ru(bpz)_3^{2+}$–Y has corresponding values of 595 nm and 4.1×10^5 s^{-1}.

With regard to the pre-exponential factors associated with the thermally activated decay (i.e., the k_2 value), the extracted values also appear to be consistent with trends noted for these parameters. Thus, Meyer and co-workers[31] have pointed out a correlation of k values with ΔE, most of the data coming from complexes exhibiting dd state domination of the thermally activated term. While but few examples were available for complexes exhibiting so-called "fourth ^{3}MLCT state" dominance, they too appeared to fall within the correlation. Briefly, a plot of $\log(k)$ vs ΔE [where ΔE is the energy gap between the lowest lying ^{3}MLCT state and either the dd^3 state ($\sim$3000 cm^{-1}) or the upper MLCT state (400–800 cm^{-1})] indicates that an increase in ΔE of approximately 100 cm^{-1} (i.e., 800 to 900 cm^{-1}) should lead to a corresponding increase in k_r by a factor of 1.7. In the case of the zeolite-entrapped complexes, there is qualitative agreement with this concept. Thus, in the case of $Ru(bpy)_3^{2+}$–Y, ΔE_2 is 890 cm^{-1} ($k_2 = 11 \times 10^7$) whereas for $Ru(bpy)_2(dmb)^{2+}$–Y the corresponding values are $\Delta E_2 = 777$ cm^{-1} and $k_2 = 6.8 \times 10^7$ (i.e., the ratio of the k values in 1.6). A similar change (though much larger) is noted for the bpz-containing complexes where the corresponding values are 895 cm^{-1} (19×10^7) for $Ru(bpy)_2(bpz)^{2+}$ and 765 cm^{-1} (1×10^7) in the case of $Ru(bpz)_3^{2+}$–Y.

F. Photophysical and Photochemical Implications. The present study demonstrates that entrapment of RuL_3^{2+} and $RuL_nL'_{3-n}^{2+}$ complexes within the zeolite supercages prevents population of the ^{3}dd state as a consequence of increases in the energy of this state which result from steric restrictions on Ru–N bond elongation. This effect has two important consequences. Obviously, it may lead to increases in the room temperature lifetime, but perhaps more importantly, it eliminates the serious problem of photodecomposition (deligation) of these complexes which proceeds through thermal population of the ^{3}dd states.

Acknowledgment. This work was supported by a grant from the Department of Energy, Office of Basic Energy Sciences (Grant ER13619). Such support does not constitute an endorsement by D.O.E. of the views expressed in this work. The authors thank Ms. Shelly M. Treffert-Zemelis for providing a sample of $Ru(mmb)_3^{2+}$.